



Synthesis and characterization of zirconia–magnesia inert matrix fuel: Ce homolog studies

Kiel Holliday*, Thomas Hartmann, Ken Czerwinski

Harry Reid Center for Environmental Studies, University of Nevada, Las Vegas, United States

ARTICLE INFO

Article history:

Received 29 August 2008

Accepted 17 April 2009

ABSTRACT

X-ray powder diffraction, microscopy, thermal analysis and electron probe microanalysis were used to characterize a ZrO₂–MgO inert matrix containing CeO₂ as a homolog for PuO₂ and Er₂O₃ as a burnable poison. The synthesis was carried out using a precipitation method. A large composition range of MgO to ZrO₂ was evaluated to determine phases present, phase mixing, phase composition, microstructure and thermal properties. It was found that most compositions of the material consist of two phases: MgO (periclase) and ZrO₂ (cubic zirconia). The zirconia phase incorporates 5% (wt/wt) MgO and up to 14% and 12% (wt/wt) CeO₂ and Er₂O₃, respectively. The MgO phase remains pure, which will enable it to retain its heat transfer and solubility properties and will improve the overall thermal conductivity and reprocessing component of the inert matrix fuel. The results with Ce will be used as the basis of future studies with actinides.

Published by Elsevier B.V.

1. Introduction

There has been a recent resurgence of interest in various oxide fuel types as potential advanced fuel for nuclear energy systems, often highlighting the role of transuranic elements as the fissile component. Inert fuel matrices have the advantage of burning transuranic elements from the fuel cycle without the additional production of plutonium [1–3]. Competitive methods for plutonium destruction include mixed oxide fuels that contain uranium. This can increase proliferation resistance by altering the plutonium isotopics, but does not significantly reduce the radiotoxicity of the spent nuclear fuel [4] or the net amount of plutonium. Neutronic calculations indicate that up to 83% of the loaded plutonium can be burnt in a uranium free fuel [5,6]. This fuel incorporates a neutron transparent inert matrix to volumetrically dilute the fissile component. The fuel must also be compatible with reactor materials such as cladding and coolant water. Additionally, a new fuel must be proliferation resistant, correspond to current safeguards and environmental safety, be economically viable, and compatible with proposed fuel recycling schemes [1,7].

One of the most widely studied candidate inert matrix materials is cubic zirconia. It is highly radiation tolerant and compatible with reactor materials [2,3,8–12]. Zirconia is suited to structurally incorporate fissile material and burnable poisons within desired compositional ranges. Cubic zirconia does not, however, possess appropriate heat transfer properties which can result in unacceptably high centerline fuel temperatures. To compensate for this, a

second phase such as MgO may be added to improve thermal diffusivity, thermal conductivity [13,14], as well as solubility for reprocessing. Pure MgO undergoes hydrolysis and subsequent swelling in the event of a cladding failure, so it cannot be used as an inert matrix fuel by itself. Zirconia is required for chemical stability [13,15].

Static corrosion experiments with pressurized water at a temperature of 300 °C have demonstrated that the addition of ZrO₂ exponentially decreases the corrosion rate of material in the zirconia–magnesia system [15]. The thermal conductivity of the zirconia–magnesia composite is greater than that of UO₂ making it suitable for current reactor safety guidelines with respect to centerline temperatures [16]. However, further study of this material is needed to better understand the limitations of isomorphic substitution within the zirconia–magnesia matrix containing a fissile component and burnable poisons [17] as well as the interaction of the material with solutions under reactor, repository, and reprocessing conditions.

The research presented in this paper examines the phases and chemical composition of Ce, Er and the inert matrix. Thermal gravimetric analysis, differential scanning calorimetry, X-ray powder diffraction, optical microscopy and electron probe microanalysis were used to determine the phases present, phase mixing, phase composition, microstructure and thermal properties. It employs CeO₂ as a homolog for PuO₂ and Er₂O₃ as a burnable poison. CeO₂ is believed to be a suitable structural homolog for PuO₂ because of the same oxidation state and similar atomic radii of 185 pm for cerium and 175 pm for plutonium. However, it is expected to be a poor chemistry homolog due to the limited oxidation states of cerium when compared to plutonium. However,

* Corresponding author.

E-mail address: kielholliday@cox.net (K. Holliday).

plutonium does remain in the 3⁺ and 4⁺ oxidation states in ceramic oxides such as MOX and will not undergo oxidization to 6⁺ in dry annealing procedures typical for its use in a nuclear reactor. The synthesis and characterization of these ceramics are the initial step in studies on the chemical behavior of inert matrix fuel under reprocessing, reactor, and repository conditions. Future studies will be aimed at exploring the chemical differences between cerium and uranium as homologs for plutonium as the actual fissile component under these conditions.

2. Experimental details

2.1. Ceramic fabrication

The precipitation method was chosen for ceramic fabrication because less severe sintering temperatures and times were required to produce a homogenous sample. Concentrated aqueous nitrate salt solutions of zirconium (Zr(NO₃)₂), magnesium (Mg(NO₃)₂), cerium (Ce(NO₃)₄), and erbium (Er(NO₃)₃) were prepared. These solutions were mixed in appropriate proportions and the metals coprecipitated with an ammonia hydroxide solution saturated with ammonium oxalate. All chemicals are reagent grade purchased from Aldrich. The precipitate was filtered and washed with purified water and acetone to remove excess ammonia. The resulting oxy-hydroxide precipitate was dried in an oven at 105 °C for 24–48 h. The dry precipitate was then ground by mortar and pestle to a powder before being calcined at 700 °C overnight in air to convert it to the oxide. The oxide powder was mixed with 1–2% (wt/wt) zinc stearate as a binder and cold pressed at 500–600 MPa with a SPEX Carver hydraulic press in a SPEX 13 mm die to produce pellets. These pellets were then sintered at 1600 °C in a Reetz LORA tube furnace for 10 h under argon atmosphere.

Cerium oxide (CeO₂) content in the ceramics varied from 3.5% to 10.5% (wt/wt) as this is within the likely range of fissile material to be incorporated into an inert matrix fuel [18]. Neutronic calculations have shown an optimal volume ratio of burnable poison to be half of the fissile phase [18]. Because of this, the erbium oxide (ErO_{1.5}) content was varied from 2.2% to 6.6% (wt/wt). The inert matrix was composed of zirconium oxide and magnesium oxide and was varied from being exclusively zirconium oxide to being completely magnesium oxide over 10 compositions (Table 1).

2.2. Thermal gravimetric analysis and differential scanning calorimetry (TGA/DSC)

An oxy-hydroxide sample of Zr_{0.866}Mg_{0.093}Ce_{0.026}Er_{0.014}O_{1.90} was prepared by precipitation of nitrate salts with base as described above. The precipitate was then dried at 80 °C overnight and ground to a powder with a mortar and pestle. A 15 mg sample of the dried oxy-hydroxide precipitate was placed in an alumina

crucible with lid. This was analyzed by a Netzsch STA 449 C Jupiter TGA/DSC under Ar atmosphere and heated from 20 to 1000 °C.

2.3. X-ray diffraction (XRD)

Sintered pellets were ground to a powder and 10 mg were mixed with 2–4 mg of silicon standard (NIST SRM 640c) as an internal reference. The internal standard allows for correcting sample displacement and goniometer off-set. This mixture was spread in a thin layer over a low-background sample holder (single crystal silicon wafer) with the aid of methanol. The analysis was performed on a PANalytical X'pert Pro diffractometer, which uses a Cu anode with Ni filter (wavelength Kα₁ at 0.1540598 nm and Kα₂ at 0.1544426 nm) and a fast multiple-Si-strip solid state detector (X'Celerator). Patterns were taken using 40 mV and 40 mA from 10° to 120° 2θ with a step size of 0.0083556° 2θ and 50.165 s per step. Phases were identified using PANalytical X'pert High Score Plus. Bruker-AXS TOPAS2 was then used to perform the least-square lattice parameter refinement and Rietveld analysis. Structure input parameters were taken from Inorganic Crystal Structure Database (ICSD). Instrument parameter inputs were as follows: primary radius (mm) 240, secondary radius (mm) 240, receiving slit width (mm) 0.1, divergence angle (°) 1, filament length (mm) 10, sample length (mm) 20, receiving slit length (mm) 30, primary sollers (°) 2.3 and secondary sollers (°) 2.3.

2.4. Optical microscopy and electron probe microanalysis

Pellets were vacuum mounted with Struers Epofix resin. Sample mounts were then ground and polished to a mirrored finish (1 μm) using a Struers TegraPol-15. Pellets were imaged using a Leica DM inverted reflectance microscope equipped with a digital Leica DFC 480 camera. After imaging the pellets, they were carbon coated and analyzed with a Joel JXA 8900R electron probe microanalyzer. Elemental mapping was done over 4 mm² at 15 keV and 100 nanoamps. Quantitative measurements were performed at 15 keV and 30 nanoamps.

3. Results and discussion

3.1. Synthesis and thermal gravimetric analysis/differential scanning calorimetry (TGA/DSC)

The TGA/DSC analysis shows that the oxy-hydroxide precipitate is converted to the oxide at 262 °C through an exothermic reaction accompanied by mass loss. The monoclinic to tetragonal phase transformation of the zirconia solid solution is indicated at 510 °C by an exothermic reaction (Fig. 1). The calcination process at 700 °C for eight hours promotes complete solid solution formation, as there is no evidence of cerium or erbium oxide starting material by XRD (Fig. 2). This isomorphous substitution is diffusion controlled. This shows solid solution formation at less severe temperatures and times than the corresponding dry synthesis route. It also provides guidance for suitable calcining temperatures and durations.

3.2. X-ray diffraction (XRD)

X-ray diffraction shows that in absence of MgO the rather small amount of CeO₂ and Er₂O₃ can only partially stabilize a fraction of the ZrO₂. As a result, a two phase mixture of monoclinic ZrO₂ (baddeleyite) and partially stabilized tetragonal ZrO₂ was identified (Fig. 2). As little as 3% (wt/wt) MgO results in fully stabilizing the cubic zirconia phase (Fig. 3). Because of this, samples with a high stoichiometric amount of Zr, (Zr_{0.866}Mg_{0.093}Ce_{0.026}Er_{0.014}O_{1.90} and Zr_{0.771}Mg_{0.188}Ce_{0.026}Er_{0.014}O_{1.80}) contain only a single cubic

Table 1
Oxide concentrations in the synthesized ceramics% (wt/wt).

Sample #	% ZrO ₂	% MgO	% CeO ₂	% ErO _{1.5}
1	94.3	0.0	3.5	2.2
2	90.7	3.2	3.8	2.3
3	86.5	6.9	4.1	2.5
4	81.4	11.3	4.4	2.8
5	75.4	16.7	4.9	3.1
6	67.9	23.2	5.5	3.4
7	58.6	31.4	6.2	3.9
8	46.5	42.0	7.1	4.4
9	30.3	56.3	8.3	5.2
10	0.0	82.9	10.5	6.6

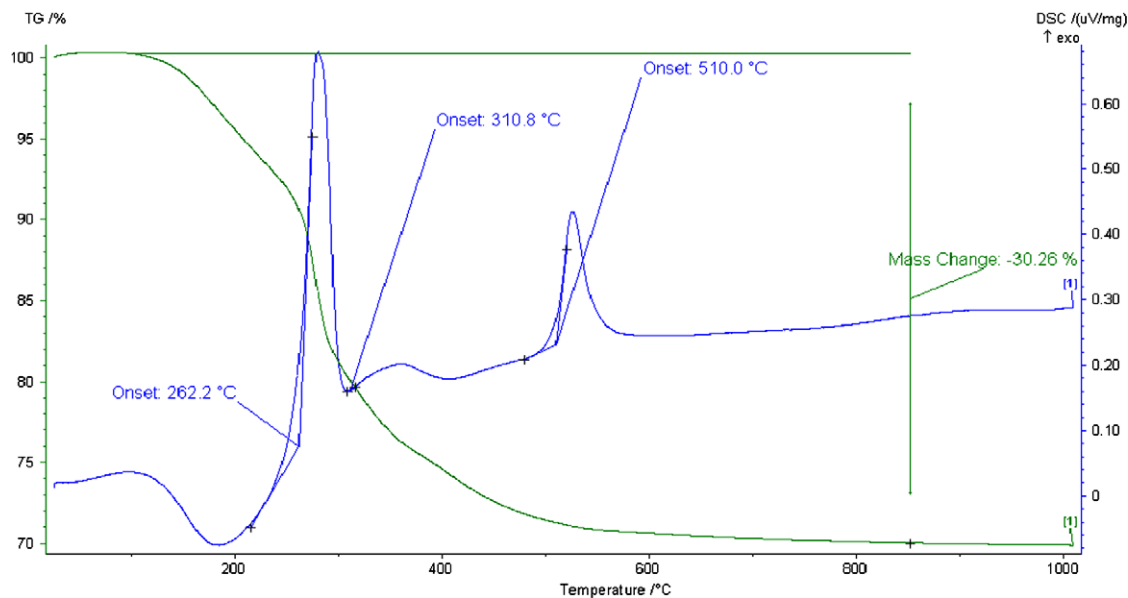


Fig. 1. Thermal gravimetric analysis and differential scanning calorimetry of precipitated material.

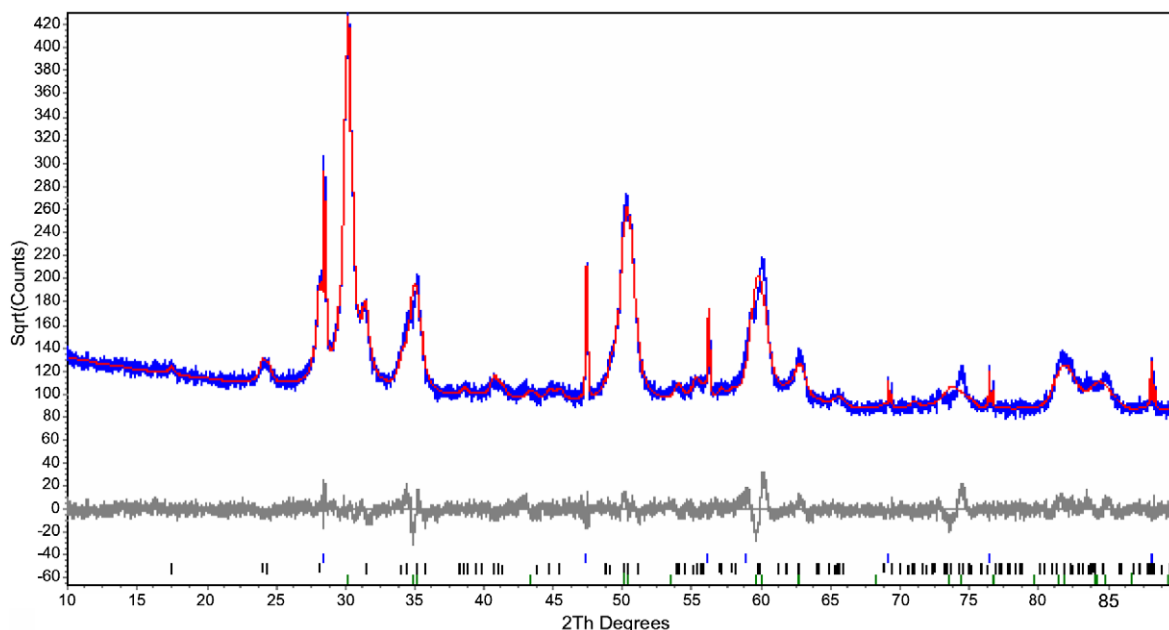


Fig. 2. X-ray diffraction pattern of calcined $Zr_{0.960}Ce_{0.025}Er_{0.014}O_{1.99}$ (blue) with fit (red) and difference curve (grey). (For interpretation of the references to colour in this figure legend, the reader is referred to the web version of this article.)

zirconia phase. If the amount of MgO is increased to 11.3% (wt/wt), MgO precipitates out of zirconia as periclase, because the solubility limit of magnesium oxide in zirconia has been exceeded under these conditions (Fig. 4). The periclase continues to build in until the ZrO_2 concentration is too low to accommodate the level of CeO_2 and Er_2O_3 that is in the sample; nominally around 30% (wt/wt) of ZrO_2 at CeO_2 and Er_2O_3 levels of 8.3% and 5.2% (wt/wt), respectively. At sufficiently low levels of ZrO_2 , CeO_2 together with Er_2O_3 form a cubic solid solution resulting in a third phase observed in sample $Zr_{0.143}Mg_{0.813}Ce_{0.028}Er_{0.016}O_{1.18}$ (Fig. 5). This CeO_2 and Er_2O_3 phase is also present when there is no ZrO_2 ($Mg_{0.956}Ce_{0.028}Er_{0.016}O_{1.04}$). A list of the phases present, lattice parameter, and quantity of each phase for each sample is in Table 2. The lattice parameter for the periclase is unchanged by the com-

position, which suggests that none of the larger cations are being incorporated into the periclase crystal structure. In contrast the more CeO_2 and Er_2O_3 in the sample the larger the unit cell of the cubic zirconia, indicating the progress in solid solution formation and the associated incorporation of Ce^{4+} and Er^{3+} cations into the zirconia lattice.

3.3. Optical microscopy and electron probe microanalysis

Optical microscopy shows zirconia as a light grey phase and periclase as a dark grey phase in reflectance permitting the identification of small quantities of MgO which may be concentrated in the grain boundaries in samples containing as little as 3% (wt/wt) MgO (Fig. 6). MgO was not identified by XRD in that sample, as

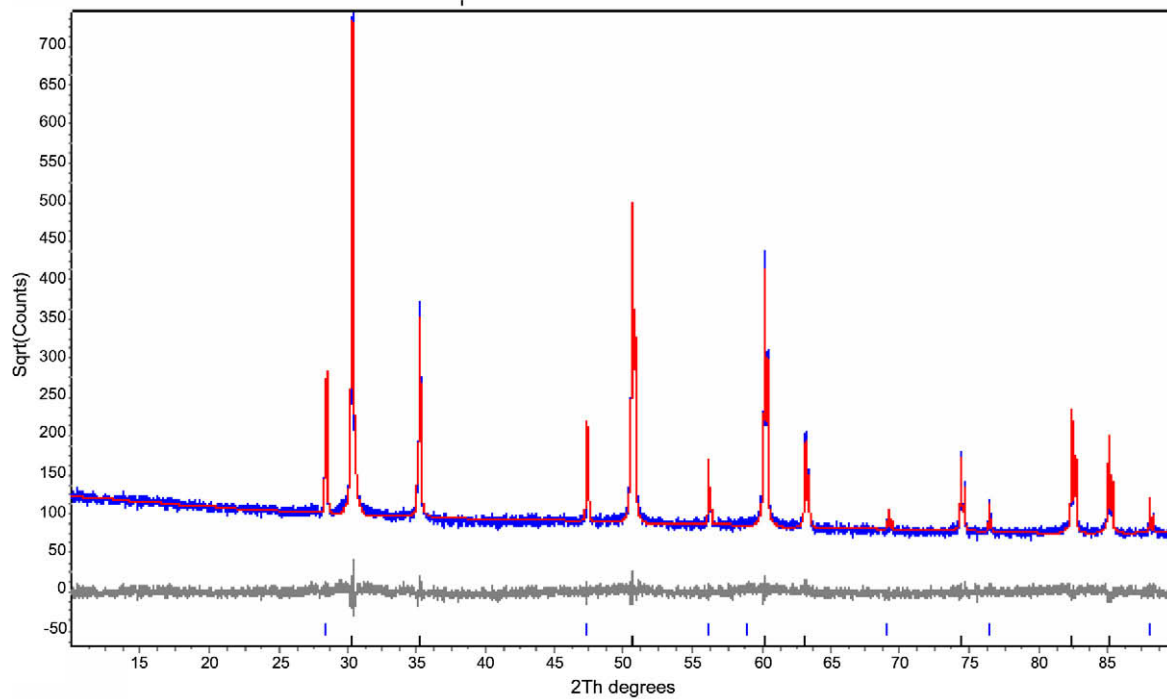


Fig. 3. X-ray diffraction pattern of sintered $Zr_{0.866}Mg_{0.093}Ce_{0.026}Er_{0.014}O_{1.90}$ (blue) with fit (red) and difference curve (grey). (For interpretation of the references to colour in this figure legend, the reader is referred to the web version of this article.)

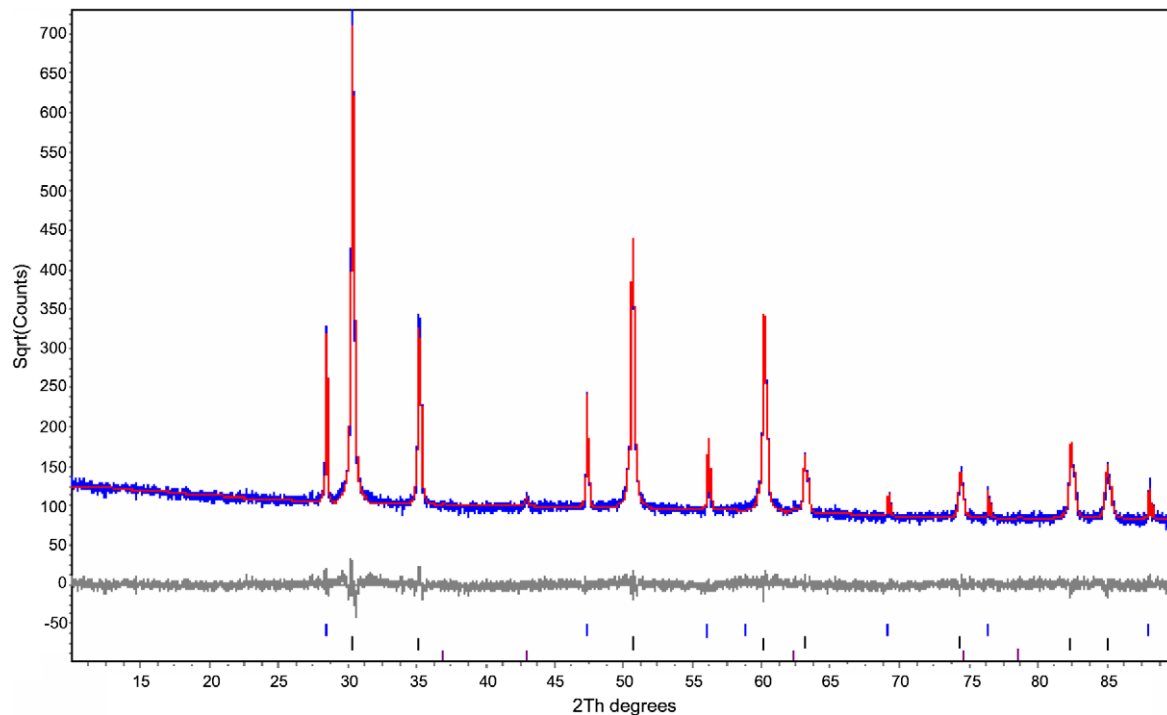


Fig. 4. X-ray diffraction pattern of sintered $Zr_{0.673}Mg_{0.286}Ce_{0.026}Er_{0.015}O_{1.71}$ (blue) with fit (red) and difference curve (grey). (For interpretation of the references to colour in this figure legend, the reader is referred to the web version of this article.)

its concentration is either below the detection limit of XRD (typically 0.1 wt%) or X-ray amorphous. It is believed that a small amount of MgO is incorporated into grain boundaries and goes undetected by X-ray diffraction. By optical microscopy it was possible to illustrate the intimate mixing of the two phases periclase and zirconia (Fig. 7).

Electron probe microanalysis was used to scan a 4 mm^2 area and to map the relative concentrations of the cations within the sample. The elemental zirconium, cerium, and erbium maps are identical indicating that cerium and erbium are evenly distributed within the zirconia phase. The magnesium map shows a faint outline of the zirconium map suggesting that a small amount of Mg is

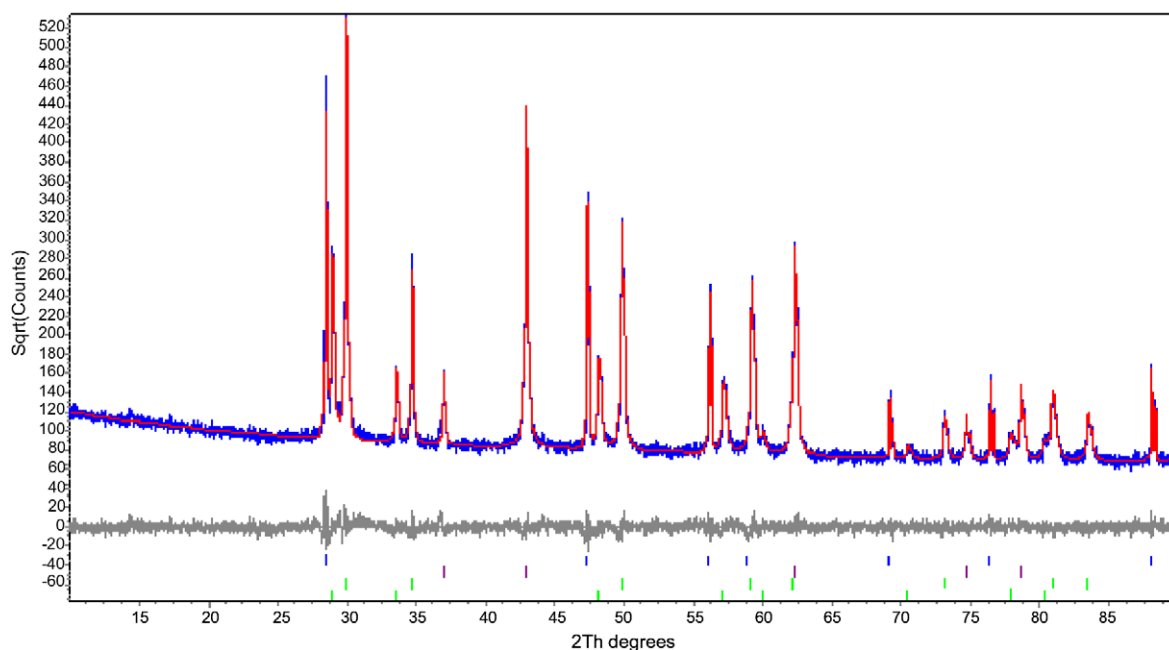


Fig. 5. X-ray diffraction pattern of sintered $Zr_{0.143}Mg_{0.813}Ce_{0.028}Er_{0.016}O_{1.18}$ (blue) with fit (red) and difference curve (grey). (For interpretation of the references to colour in this figure legend, the reader is referred to the web version of this article.)

Table 2

Phases present and lattice parameters as determined by XRD.

Sample #	Bulk sample composition (calculated)	Phases present (space group)	Lattice parameters (nm)	Stoichiometry of phase as determined by EPMA	Quantity (wt%)
1	$Zr_{0.960}Ce_{0.025}Er_{0.014}O_{1.99}$	ZrO_2 ($P12_1/c1$)	0.51585(2) 0.52123(7) 0.53341(8)	Not determined	27.0
		ZrO_2 ($P42/nmcS$)	0.36397(10) 0.50966(7)	Not determined	73.0
2	$Zr_{0.866}Mg_{0.093}Ce_{0.026}Er_{0.014}O_{1.90}$	ZrO_2 ($Fm-3m$)	0.50964(5)	$Zr_{0.892}Mg_{0.075}Ce_{0.019}Er_{0.014}O_{1.92}$	100.0
3	$Zr_{0.771}Mg_{0.188}Ce_{0.026}Er_{0.014}O_{1.80}$	ZrO_2 ($Fm-3m$)	0.50978(3)	$Zr_{0.814}Mg_{0.141}Ce_{0.029}Er_{0.014}O_{1.85}$	100.0
4	$Zr_{0.673}Mg_{0.286}Ce_{0.026}Er_{0.015}O_{1.71}$	ZrO_2 ($Fm-3m$)	0.50988(5)	$Zr_{0.834}Mg_{0.112}Ce_{0.036}Er_{0.017}O_{1.88}$	98.3
		MgO ($Fm-3m$)	0.42135(4)	MgO	1.7
5	$Zr_{0.571}Mg_{0.387}Ce_{0.027}Er_{0.015}O_{1.61}$	ZrO_2 ($Fm-3m$)	0.51113(8)	$Zr_{0.792}Mg_{0.143}Ce_{0.044}Er_{0.021}O_{1.85}$	83.7
		MgO ($Fm-3m$)	0.42139(3)	MgO	16.3
6	$Zr_{0.468}Mg_{0.489}Ce_{0.027}Er_{0.015}O_{1.50}$	ZrO_2 ($Fm-3m$)	0.51156(5)	$Zr_{0.774}Mg_{0.152}Ce_{0.049}Er_{0.025}O_{1.84}$	62.6
		MgO ($Fm-3m$)	0.42129(9)	MgO	37.4
7	$Zr_{0.363}Mg_{0.594}Ce_{0.027}Er_{0.016}O_{1.40}$	ZrO_2 ($Fm-3m$)	0.51202(9)	Not determined	55.8
		MgO ($Fm-3m$)	0.42126(4)	Not determined	44.2
8	$Zr_{0.254}Mg_{0.702}Ce_{0.028}Er_{0.016}O_{1.29}$	ZrO_2 ($Fm-3m$)	0.51516(9)	$Zr_{0.722}Mg_{0.139}Ce_{0.094}Er_{0.045}O_{1.84}$	43.4
		MgO ($Fm-3m$)	0.42125(10)	MgO	56.6
9	$Zr_{0.143}Mg_{0.813}Ce_{0.028}Er_{0.016}O_{1.18}$	ZrO_2 ($Fm-3m$)	0.51747(10)	$Zr_{0.682}Mg_{0.118}Ce_{0.114}Er_{0.086}O_{1.84}$	20.5
		MgO ($Fm-3m$)	0.42125(8)	Mgo	72.6
10	$Mg_{0.956}Ce_{0.028}Er_{0.016}O_{1.04}$	$Ce_xEr_yO_{2x+1.5y}$ ($Fm-3m$)	0.53419(9)	Not determined	6.9
		MgO ($Fm-3m$)	0.42119(8)	MgO	87.7
		$Ce_xEr_yO_{2x+1.5y}$ ($Fm-3m$)	0.54342(6)	Not determined	12.3

contained within the zirconia phase. However, in samples containing a secondary periclase phase there are also high concentrations of magnesium in areas that have, besides oxygen, no other elements present. This shows that the periclase is relatively pure MgO, which is also consistent with the results of the periclase lattice parameter refinement from the XRD powder data.

Microprobe analysis was also used to quantify the amount of each element present in small volumes. In this way the stoichiometry of each phase within a sample was examined. In the zirconia phase, there is an increase in MgO content as MgO in the sample is increased from 0% to 11% (wt/wt) in the total sample. At this point the cubic zirconia is saturated with respect to MgO. The zirconia phase contains up to 5% (wt/wt) MgO at saturation, and any

increase in MgO in the sample has no effect on the MgO content of the ZrO_2 phase. It can be stated that the solubility limit of Mg for cubic stabilized zirconia is 5% (wt/wt) under these conditions. The amount of cerium and erbium continues to grow as more cerium and erbium are added to the ceramic. The maximum amount of cerium and erbium was 14% and 12% (wt/wt), respectively for sample $Zr_{0.143}Mg_{0.813}Ce_{0.028}Er_{0.016}O_{1.18}$, in which a cerium erbium oxide phase began to precipitate (Fig. 8). It was difficult to probe the periclase phase in many samples due to the small area and intimate mixture of the phases. However, many measurements show less than 1% (wt/wt) of any other species in the periclase, again supporting earlier data suggesting low affinity of cerium, erbium, and zirconium for isomorphous substitution or for occupying inter-

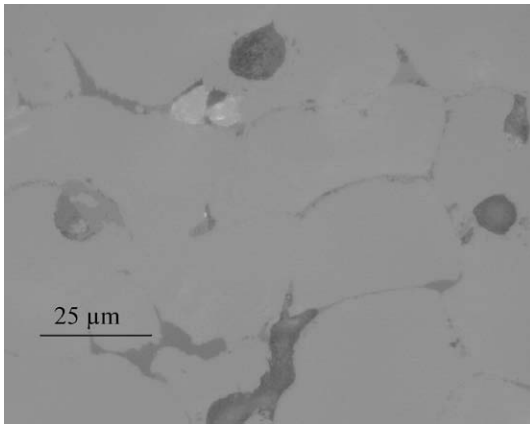


Fig. 6. Optical microscope image of $Zr_{0.866}Mg_{0.093}Ce_{0.026}Er_{0.014}O_{1.90}$ 1000 \times magnification. Zirconia-based fuel phase (grey) and pore space (dark) with MgO material incorporated into grain boundaries (dark grey).

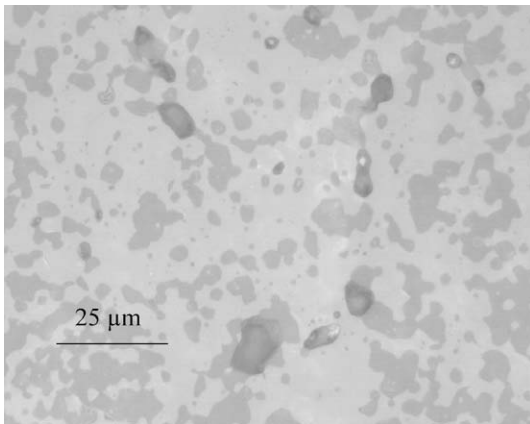


Fig. 7. Optical microscope image of $Zr_{0.468}Mg_{0.489}Ce_{0.027}Er_{0.015}O_{1.50}$ 1000 \times magnification. Zirconia-based fuel phase (light grey) and periclase phase (dark grey) with some pore space (dark).

stitials within this phase. A summary of this data can be found in Table 2. It should be noted that the discrepancy between the calculated stoichiometry and measured phase stoichiometry can be accounted for by amorphous MgO accumulating in grain boundaries as was seen by optical microscopy (Fig. 6).

4. Conclusion

The precipitation method used to synthesize zirconia magnesia inert matrix fuels has been used to produce dual phase material with intimate mixing between phases. It has also been shown to form a solid solution at less severe temperatures (510 °C) and durations than the corresponding dry synthesis route as demonstrated by TGA/DSC. This could be beneficial for burning higher actinides with low sublimation temperatures, such as americium. The ZrO_2 requires very little MgO in the presence of CeO_2 and Er_2O_3 to fully stabilize the cubic zirconia phase. This zirconia phase can accommodate up to 14% (wt/wt) fissile material and up to 12% (wt/wt) burnable poison. A consistent 5% (wt/wt) MgO is contained in the zirconia phase allowing for a reliable estimate of the quantity of the periclase that will be present for a given composition. The relative amount of Mg is found to determine the phase composition of the resulting material. With no MgO, ZrO_2 is in both baddeleyite and tetragonal phases. As little as 3.2% (wt/wt) and as much as 6.9% (wt/wt) MgO resulted in a single cubic zirconia phase. A periclase phase precipitated at MgO concentrations above 10% (wt/wt) MgO. A third phase of cubic Ce–Er oxide was found after exceeding the solubility limit of the zirconia. This was found at ZrO_2 concentration of 30% (wt/wt) with Ce and Er concentrations of 8.3% and 5.2% (wt/wt), respectively. This phase is also present in the absence of zirconia. The periclase remains pure which will allow it to retain its thermophysical properties, most importantly thermal diffusivity and thermal conductivity, and to further improve the reactor-related qualities of the overall ceramic. This characterization study was performed to lay a foundation for dissolution studies of zirconia–magnesia inert matrix fuel under conditions of interest. These experiments will be performed with uranium and plutonium in future studies, providing detailed comparison on the suitability of cerium as a structural plutonium homolog and identifying trends associated with the fissile component of the inert matrix fuel.

Acknowledgements

The authors would like to thank Robert Fairhurst for his expertise with the microprobe. This project was funded under the UNLV Transmutation Research Program administered by the Harry Reid Center for Environmental Studies under the auspices of the US Department of Energy, Office of Nuclear Energy (Cooperative Agreement No. DE-FG07-01AL67358).

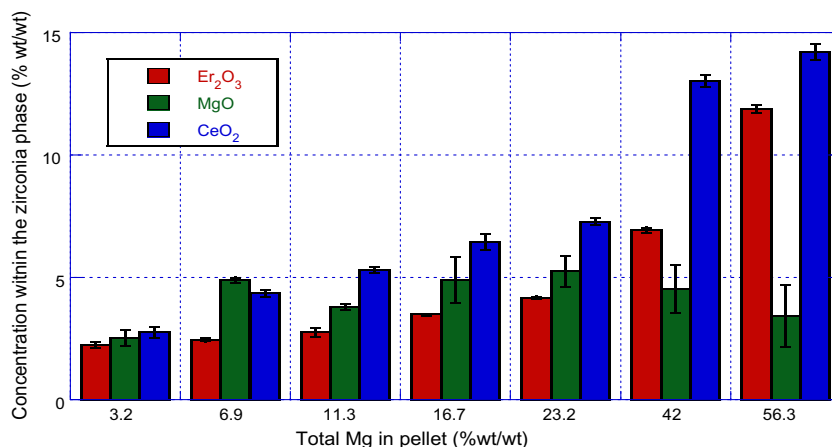


Fig. 8. Stoichiometry of the zirconia phase by electron probe microanalysis. (Error bars represent standard deviation in measurements.)

References

- [1] W.J. Carmack, M. Todosow, M.K. Meyer, K.O. Pasamehmetoglu, *J. Nucl. Mater.* 352 (2006) 276.
- [2] R. Chawla, R.J.M. Konings, *Progr. Nucl. Energy* 38 (2001) 455.
- [3] G. Ledergerber, C. Degueldre, P. Heimgartner, M.A. Pouchon, U. Kasemeyer, *Progr. Nucl. Energy* 38 (2001) 301.
- [4] A. Shelley, H. Akie, H. Takano, H. Sekimoto, *Progr. Nucl. Energy* 38 (2001) 439.
- [5] C. Lombardi, A. Mazzola, *Ann. Nucl. Energy* 23 (1996) 1117.
- [6] C. Lombardi, A. Mazzola, E. Padovani, M.E. Ricotti, *J. Nucl. Mater.* 274 (1999) 181.
- [7] C. Degueldre, J.M. Paratte, *J. Nucl. Mater.* 274 (1999) 1.
- [8] G. Curran, W. Rattray, K.R. Czerwinski, *Radiochim. Acta* 91 (2003) 203.
- [9] G. Curran, Y. Sevestre, W. Rattray, P. Allen, K.R. Czerwinski, *J. Nucl. Mater.* 323 (2003) 41.
- [10] C. Degueldre, S. Conradson, *Appl. Phys. A: Mater. Sci. Process.* 73 (2001) 489.
- [11] N. Kamel, H. Ait-Amar, M. Taouinet, C. Benazzouz, Z. Kamel, H. Fodil-Cherif, S. Telmoune, R. Slimani, A. Zahri, D. Sahel, *Progr. Nucl. Energy* 48 (2006) 70.
- [12] F. Vettraino, G. Magnani, T. La Torretta, E. Marmo, S. Coelli, L. Luzzi, P. Ossi, G. Zappa, *J. Nucl. Mater.* 274 (1999) 23.
- [13] P. Medvedev, Dissertation, Texas A&M University, 2004.
- [14] C. Ronchi, J.P. Ottaviani, C. Degueldre, R. Calabrese, *J. Nucl. Mater.* 320 (2003) 54.
- [15] P.G. Medvedev, S.M. Frank, T.P. O'Holleran, M.K. Meyer, *J. Nucl. Mater.* 342 (2005) 48.
- [16] P.G. Medvedev, M.J. Lambregts, M.K. Meyer, *J. Nucl. Mater.* 349 (2006) 167.
- [17] P.G. Medvedev, J.F. Jue, S.M. Frank, M.K. Meyer, *J. Nucl. Mater.* 352 (2006) 318.
- [18] E. Fridman, E. Shwageraus, *Nucl. Technol.* 157 (2) (2007) 157.